NUMERICAL INVESTIGATION OF COHERENT STRUCTURES FORMING AROUND BRIDGE PIERS SITTING ON AN INCLINED SURFACE

A THESIS SUBMITTED TO
THE GRADUATE SCHOOL OF NATURAL AND APPLIED SCIENCES
OF
MIDDLE EAST TECHNICAL UNIVERSITY

BY

EMRE HESAP

IN PARTIAL FULFILLMENT OF THE REQUIREMENTS
FOR
THE DEGREE OF MASTER OF SCIENCE
IN
CIVIL ENGINEERING

NOVEMBER 2021

Approval of the thesis:

NUMERICAL INVESTIGATION OF COHERENT STRUCTURES FORMING AROUND BRIDGE PIERS SITTING ON AN INCLINED SURFACE

submitted by **EMRE HESAP** in partial fulfillment of the requirements for the degree of **Master of Science** i**n Civil Engineering, Middle East Technical University** by,

Prof. Dr. Halil Kalıpçılar
Dean, Graduate School of **Natural and Applied Sciences** _____

Prof. Dr. Ahmet Türer
Head of the Department, **Civil Engineering** _____

Prof. Dr. Mete Köken
Supervisor, **Civil Engineering, METU** _____

Examining Committee Members:

Prof. Dr. İsmail Aydın
Civil Eng., METU _____

Prof. Dr. Mete Köken
Civil Eng., METU _____

Assoc. Prof. Dr. Elif Oğuz
Civil Eng., METU _____

Assoc. Prof. Dr. Gökçen Bombar
Civil Eng., İzmir Katip Çelebi Unversity. _____

Assoc.Prof. Dr. Müsteyde Koçyiğit
Civil Eng., Gazi University _____

Date: 05.11.2021

I hereby declare that all information in this document has been obtained and presented in accordance with academic rules and ethical conduct. I also declare that, as required by these rules and conduct, I have fully cited and referenced all material and results that are not original to this work.

Name Last name : Emre HESAP

Signature :

ABSTRACT

NUMERICAL INVESTIGATION OF COHERENT STRUCTURES FORMING AROUND BRIDGE PIERS SITTING ON AN INCLINED SURFACE

Hesap, Emre
Master of Science, Civil Engineering
Supervisor: Prof. Dr. Mete Köken

November 2021, 43 pages

Coherent structures forming around the piers play an important role in the formation of scour hole. Detached Eddy Simulation is used in this study to investigate the three-dimensional coherent structures forming around bridge piers which sit on an inclined surface. Initiation of the scour process at flat bed conditions is investigated within the current study. Two cases are investigated one with the lower Reynolds number case which is typical for flume experiments whereas the larger Reynolds number case represents the physical conditions found in nature. Also, comparison was done with a study in the literature with uninclined bed conditions. It was observed that a horseshoe vortex forms around the pier in both cases studied. Shear stress values over the bed is evaluated. As result, it was observed that high bed shear stress values occur in the acceleration regions on both sides of the pier and along the detached shear layers. In both simulations, these stresses are observed to be effective across a wider band on the shallow channel side rather than on the deep channel side. Comparing the results of this study with the literature it was concluded that inclined channels are more critical in terms of the scour formation.

Keywords: Detached Eddy Simulation,Coherent Structures, Bridge Pier

ÖZ

EĞİMLİ TABAN YÜZEYİNE OTURAN KÖPRÜ AYAKLARI ETRAFINDAKİ AKIM YAPILARININ SAYISAL OLARAK INCELENMESİ

Hesap, Emre
Yüksek Lisans, İnşaat Mühendisliği
Tez Yöneticisi: Prof. Dr. Mete Köken

Kasım 2021, 43 sayfa

Köprü ayakları etrafında oluşan akım yapıları bölgedeki oyulma çukurunun oluşumuna doğrudan etki etmektedir. Bu çalışmada, eğimli bir yüzey üzerinde oturan köprü ayakları etrafında oluşan üç boyutlu akım yapılarını incelemek için ayrışan döngü benzetimi kullanılmıştır. Bu çalışmada düz zemin koşullarında oyulma başlangıcı incelenmiştir. Çalışmada yüksek ve düşük Reynold sayısına akımlar için iki farklı durum incelenecektir. Düşük Reynold sayısına sahip akım deneysel kanal akımlarının karakteristik özelliği olup yüksek Reynold sayısına sahip durum ise doğada genellikler var olan koşullar temsil etmektedir. Ayrıca literatürdeki eğimli olmayan bir yüzeyde yapılan bir çalışmayla karşılaştırma yapılmıştır. Her iki simülasyonda köprü ayağı etrafında oluşan at nalı vortekslerinin oluştuğu gözlemlenmiştir. Simülasyonlarda yatak üzerindeki kayma gerilmesi değerleri değerlendirilecek ve bu da olası oyulma bölgeleri hakkında değerli bilgiler verecektir. Sonuç olarak köprü ayağının her iki yanındaki hızlanma bölgelerinde ve ayrışmış kesme tabakaları boyunca yüksek zemin gerilmesi değerlerinin oluştuğu gözlemlenmiştir. Bu gerilmeler her iki benzetimde de sığ kanal tarafında derin kanal tarafında göre daha geniş bir bant boyunca etkili olduğu gözlemlenmiştir. Bu

çalışmanın sonuçları literatür ile karşılaştırıldığında, oyulma oluşumu açısından eğimli kanalların daha kritik olduğu sonucuna varılmıştır.

Anahtar Kelimeler: Ayrışan döngü benzetimi, Akım yapıları, Köprü ayağı

To my family

ACKNOWLEDGMENTS

I would like to thank my supervisor Prof. Dr. Mete Köken for his guidance, advice, criticism and patience throughout the process. It was an honor to work with him. I would like to express his great dedication to this work.

I would like to thank Katip Çelebi University and Assoc.Prof.Dr. Gökçen Bombar for their works this project.

I would like to thank İlker Çoban, who was my closest and most valuable friend during my undergraduate and graduate education.

I would also like to render my sincere thanks to my family for their support and trust in me throughout all my education life.

This work is partially funded by Scientific and Technological Research Council of Turkey under grant number TUBİTAK 116M519

TABLE OF CONTENTS

LIST OF TABLES

TABLES

LIST OF FIGURES

FIGURES

LIST OF ABBREVIATIONS

ABBREVIATIONS	
DES	Detached Eddy Simulation
LES	Large Eddy Simulation
RANS	Reynolds Averaged-Navier Stokes
SA	Spalart-Allmaras

SYMBOLS

B	mean channel width
Cb1, Cb2, Cv1	Spalart Almaras model constants
Cw1, Cw2, Cw3	Spalart Almaras model constants
CDES	model constants
D	Pier width
dDES	DES length scale
f_{v1}, f_{v2}, f_w	Spalart Almaras model constants
r	Spalart Almaras model parameter
Re	Reynolds Number
Š	Spalart Almaras model parameter
t	time
V	average flow velocity
u_j	contravariant velocity component in j direction
u_j	cartesian mean velocity component in j direction
κ	Von-Karman constant
τ_w	wall shear stress
ν	kinematic viscosity
ŭ	modified eddy viscosity
ν_t	turbulent eddy viscosity
σ	Spalart Almaras model constant
χ	Spalart Almaras model parameter
y	Non-dimensional first layer thickness

ω_z	out-of-plane vorticity
Δ	local grid size

CHAPTER 1

INTRODUCTION

1.1 Background

Bridges are crucial structures for both railroads and highways to ensure the continuity of the transportation. Thus, safe and economic designs of bridges are quite significant. Statistical studies conducted to investigate the reasons of bridge failures show that majority of the bridge failures stem from extreme scouring at substructure components. Hence, a bridge which passes over a sedimentary river should be designed taking scour possibility at piers and abutments into account (Yanmaz & Apaydın, 2012). Therefore, hydraulic parameters are as important as structural parameters while designing a bridge.

Harik et al. (1990) investigated bridge failures in the United States between 1951-1988 and this investigation concluded that 29 out of a total of 79 failures were caused due to flood, scour and wind. According to Flint et al. (2017), floods, scour and other hydraulic events are the most frequent reasons of the total or partial failure of the bridges. In the United States, 20% of the bridge failures stem from the scour of the infrastructural components.

In Turkey, Çaycuma bridge failure is one of the most obvious instances of bridge failure due to scour. In 2012, Çaycuma Bridge collapsed due to bridge scour and resulted in 15 deaths (Ercan & Gündoğan, 2012).

To conclude, a true estimation of the scour depth around the bridge piers and viaducts located on the side slopes of a stream is crucial in terms of the safety and economy of the structure.

Figure 1.1 Çaycuma bridge after the collapse (Ercan & Gündoğan, 2015)

The present study has been conducted within the scope of TUBITAK 116M519 coded project. Coherent structures forming around bridge piers which sit on an inclined surface were investigated numerically. Detached Eddy Simulation was used to investigate the aforementioned three-dimensional coherent structures.

Katip Celebi University is also carrying out another study within the scope of this TUBITAK project. Channel, pier geometry and flow properties used in the study of Katip Çelebi University are used in the first case simulated within the scope of this thesis; only the channel and the pier geometry are used in the second case simulated within the scope of this thesis.

Two scenarios are tested within this thesis all having flatbed conditions which represents the initiation of the scour process. Simulations are run at two different Reynolds numbers at 52,480 and 262,400. The lower Reynolds number case (Case I) is typical for flume experiments whereas the larger Reynolds number case (Case II) represents the physical conditions found in nature. In addition, results of Kirkil

and Constantinescu's (2015) study named "*Effects of cylinder Reynolds number on the turbulent horseshoe vortex system and near wake of a surface-mounted circular cylinder"* which performed in similar conditions with case I was used and compared with the results of Case I.

Channel geometry, pier geometry and flow information are given in Table 1.1

Table 1.1 *Flow and geometric details of Case I*

	Geometric Properties						Flow Properties		
Case	**B (cm)**	**D (cm)**	**h_1 (cm)**	**h_2 (cm)**	**α**	**A (m^2)**	**Q (lt/s)**	**V (cm/s)**	**Re**
Case I	120	16	38	4	16	0.252	82.6	32.8	52480
Case II	120	16	38	4	16	0.252	413	164	262400

In table 1.1 Q represents discharge, B represents width of the flume, V represents velocity, h_1 and h_2 represents the length of the sides of the flume, D represents diameter of the pier, A represents area of the cross section and α represent angle between base of the flume and horizontal axis

Profile view of flume with geometric properties is given at the Figure 1.2 at below.

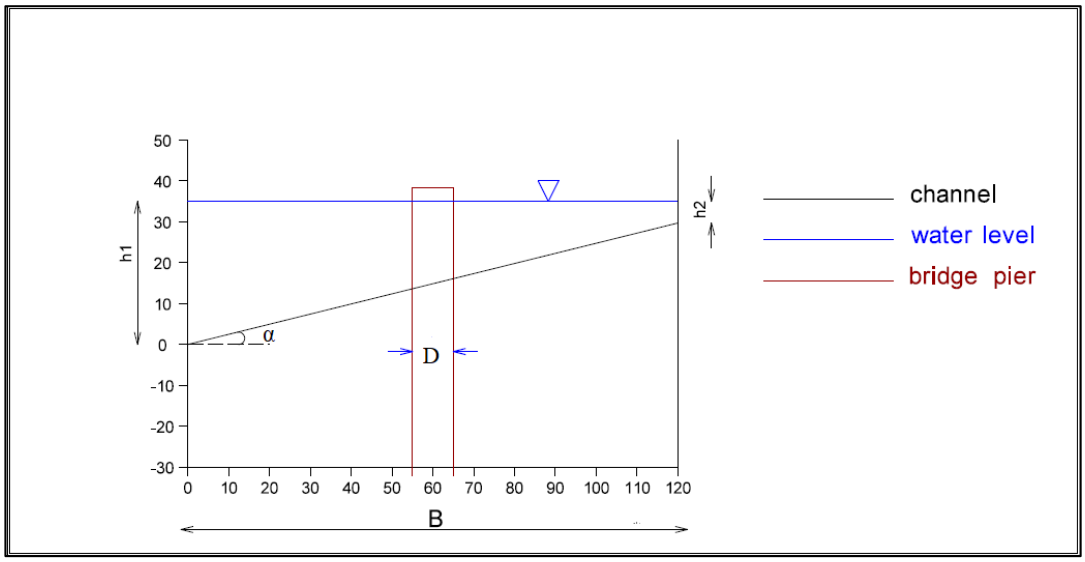

Figure 1.2. Profile view of the flume with geometric parameters

In the simulations made within the scope of the study, the Spalart Almaras-based DES (Detached Eddy Simulation) turbulence model was used. This model is a hybrid

model and regions close to walls are analyzed in RANS (Reynolds Average Navier Stokes) model, while regions far from wall are analyzed in LES (Large eddy simulation) model. DES simulations were made at two different Reynolds numbers in the non-scoured bed conditions. The Reynolds number lower than these two simulations represents the flume conditions; The higher Reynolds number is conducted to represent the situation that will actually occur in rivers. The simulations at low and high Reynolds numbers are named as Case I and Case II simulations, respectively. In the simulations, all dimensions are given by dimensioning the bridge pier diameter D. The view of the calculation area is given in Figure 1.3. In the calculations, the channel length was taken as 35D and the bridge pier was placed at a distance of 10D from the entrance section.

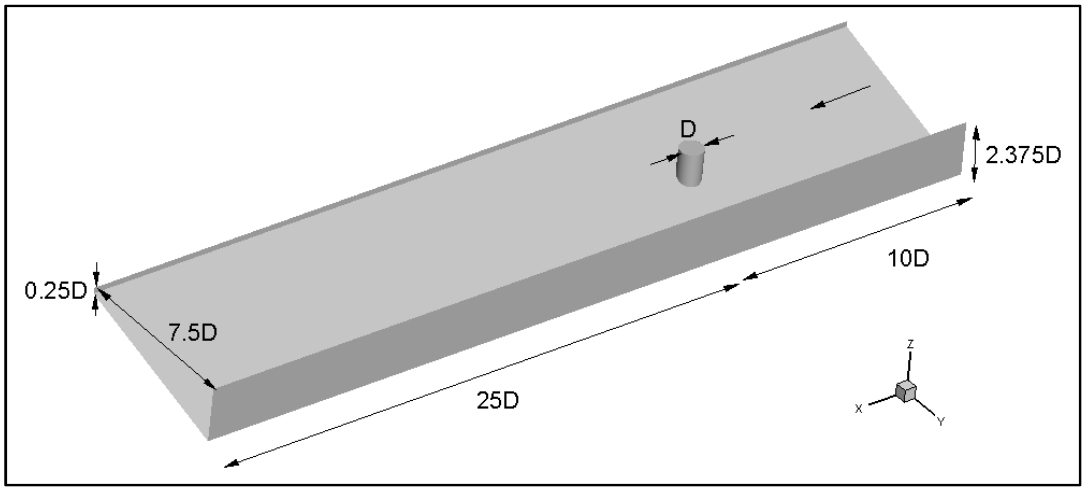

Figure 1.3. General view of study area

,

1.2 Literature Review

There are many studies on bridge piers in the literature. In this section, some numerical studies in the literature are compiled and the possible contribution of this study to the literature is explained.

Nishino, Roberts and Zhang (2008) compared their experimental work (Nishino et al,2007) with URANS and Detached Eddy simulation flow around a circular cylinder. As results DES results matched the experimental results, where URANS did not.

In Travin et al. (2000), the authors observed the flow around a cylinder in a flat-bed channel using two different Reynolds Numbers, 50,000 and 140,000 to validate Detached Eddy Simulation. In the case with a low Reynolds number, DES was much better with respect to Unsteady Reynolds Averaged Navier Stokes method. However, In the case with a high Reynolds number results were very close with URANS method. The authors indicated that further studies are necessary to validate DES for higher flow with higher Reynolds number.

Squires et al. (2008) observed the flow around a cylinder in a flat-bed condition using Detached Eddy Simulation and Delayed Detached Eddy simulation. It gave results compatible with experimental studies in both simulations.

Breuer (1998) conducted a Large Eddy simulation of flow around a cylinder in a flat-bed channel. The author's goal was not to observe the current but to find out what affects the quality of the simulation. The research showed that for the LES, the numerical distribution is more important than the sequence of correctness.

Vornom et al. (2011) conducted a Large Eddy simulation using 3 different Reynolds numbers, 3900, 10,000 and 20,000, around the cylinder, keeping other variables constant. Although the agreement with previous experimental studies is generally good, minor differences were observed in simulations with Reynolds numbers of

10,000 and 20,000. The authors showed reason this to the decreasing resolution as the Reynolds number increases.

Cheng, Koken, Constantinescu (2018) conducted a detached eddy simulation around a circular and a rectangular pier separately. Flat bed and scoured bed conditions were simulated separately. Bathymetry data was used during scoured bed condition simulations. The aim of the study is to understand coherent structures' behavior around these piers under both flat bed and scoured bed conditions. Also, RANS simulations generally underestimate the scour depth due to its inability to compute unsteady dynamics of coherent structures. Hence, a new methodology was proposed by the researchers to improve RANS results by taking into consideration of bed-friction velocity that is generally neglected in RANS. This parameter was calculated 1.5-4 by DES results and using the lower values was suggested by the researchers when time-accurate RANS simulations were conducted.

Xu, Chen and Lu (2007) conducted Large Eddy Simulation, Detached Eddy Simulation and URANS to inspect the turbulent stream nearby a cylindrical pier. The aim of the study is to make clear to the application of these models on the cylindrical pier. Spalart-Allmaras (SA), Subgrid Scale (SGS) and Shear-Stress-Transport (SST) models were used in simulations. The average pressure coefficient and drag coefficient, velocity profile, Strouhal number, and Reynolds stress are the results obtained in comparison with previous numerical and experimental information. The capacity and efficiency of these simulation methods, as well as the related turbulence model, were assessed based on comprehensive simulations in order to simulate the separate turbulent flow.

Kirkil, Constantinescu and Ettema (2009) conducted detached eddy simulation to solve dynamics of eddies around a circular pier. The aim of this study is to examine the subtleties of the coherent structures, their transactions, and their function on sediment transportation scour hole formed. 2.06×10^5 was used as Reynolds number. Also, a comparison was done with the researchers' previous study in which Reynold's number is 16.000. At the study, the researchers posed the analysis of the

mechanism of the horseshoe vortices and wake vortices. At the stages of the phases process creation of the downflow at the upstream of the pier, which is very important for the forming of the scour was deliberated. As the result of the study, similar results with both experimental studies and low Reynold's number study were obtained.

1.3 Research Objectives & Scope of the Study

It is seen that numerical studies in the literature were carried out under flatbed conditions. In this study, detached eddy simulation was conducted in inclined bed conditions. The results were compared with the study performed by Kirkil and Constantinescu (2005) under flatbed conditions and similar flow conditions and evaluated in terms of possible scour mechanisms. Also, another purpose of this study is to investigate the effect of transversal slope on the coherent structures formed around the bridge piers using Detached Eddy Simulation.For this intention, a bridge pier is simulated under two different flow conditions.

1.4 Thesis Organization

The structure of this paper is as follows. A brief introduction and literature review can be found in Chapter 1. Chapter 2 describes the main formulas for the Spalart-Allmaras based DES model used in the calculations. In addition, this chapter describes the key parameters, the numerical model, grid generation, and the computation process. In Chapter 3, The simulation results of the two simulations and comparison study are examined and compared Finally, Chapter 4 express conclusions.

CHAPTER 2

NUMERICAL MODEL

2.1 Theoretical Background

General turbulence modeling methods are explained in this chapter.

2.1.1 Direct Numerical Simulation (DNS)

Among all turbulence modeling methods, Direct numerical simulation (DNS) is the method that gives the most precise results. (Zhou,2018) In this approach, time-subordinate Navier-Stokes conditions are tackled and all connected disturbance time and length scales are settled straightforwardly with no roughness model for the stream considered under material introductory and limit condition. Indeed, even the mathematical way impacts the exactness of the arrangement itemized information about turbulence properties are required and it is hard to acquire all things considered of the investigations. In spite of the fact that DNS is the best approach for achieving a turbulent flow solution, computational costs rise quickly as for Reynolds number and DNS grids should be perfect to solve the even smallest eddies. Thus, it is only applicable to basic, low Reynolds numbers engineering applications with today's computer power.

2.1.2 Large Eddy Simulation (LES)

Large eddy simulation solves large eddies like in the DNS however, little eddies are solved by sub-gird scale models (SGS). The drawback of the large eddy simulation for engineering applications is the fine mesh resolution and modest computational requirements

2.1.3 Reynolds Averaged Navier-Stokes (RANS) Equations and Closure Models

The governing equation is disintegrated into mean and fluctuating quantities in the Reynold-averaged Navier-Stokes's equations, an additional term, the Reynolds stress tensor, arises following this decomposition and using eddy viscosity-based closure models, the effects of this tensor are modeled. From simple algebraic models to second order closure models, many closure models exist. In the books by Hofmann, Wilcox and Pope there are explanations of these closure models Turbulence prediction for most engineering applications results from solving RANS.

2.1.4 Hybrid Models

The integration of the RANS turbulence models with DNS / LES is the main purpose of hybrid models due to lower cost of computation. Near wall borders, RANS solutions are used to reduce mesh size and at the remainder of the domain DNS / LES is used in the hybrid models.

2.1.5 Partially Averaged Navier-Stokes (PANS)

The advantages of RANS and DNS models are combined in the Partially Averaged Navier-Stokes turbulence model. The control parameters are used to determine an adequate filter width in order to obtain PANS equations from the precursor RANS equations. Undissolved kinetic energy and dissipation are solved by the PANS calculations. It is also important that determination of the quantity of the kinetic energy and dissipation rate is to be modeled. the concept of PANS hybrid turbulence is explained by Sharath S. Girimaji (2005)

2.1.6 Hybrid LES-RANS Models (HLR)

To utilize both techniques of Reynolds Averaged Navier-Stokes and large eddy simulation, hybrid LES -RANS models are used. To minimize the computational cost, near the walls RANS is used and LES is used at the rest of the area. This method is known as Detached Eddy Simulation (DES). However, to deal with the gray area

problem, there are several DES models, such as Delayed Detached Eddy Simulation and the Zonal Detached Eddy Simulation.

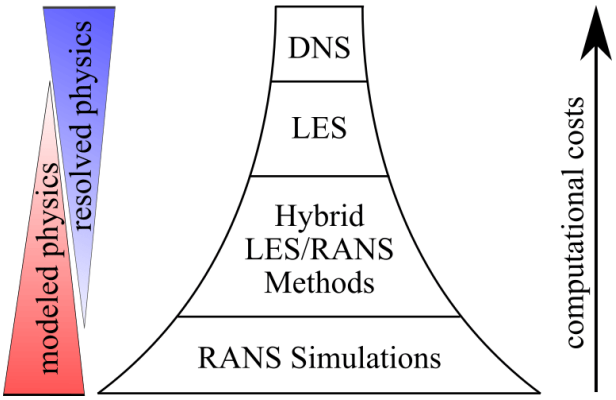

Figure 2.1: A graphical description of the hierarchy of turbulence simulation methods focused on computing costs and the amount of solved and modeled physics. (Xiao & Cinnella, 2019)

Detached-eddy simulation (DES) is presented firstly in 1997.In Detached Eddy simulation method Reynolds-Averaged Navier Stokes (RANS) technology which is effective at boundary layers and Large Eddy Simulation which is effective at separated regions come together. (Spalart, 2009) Travin et al (2000) defined DES97 which is the original version of the DES as 3D numerical solution which works as Large Eddy simulation in the well grid density zones and RANS model in the inadequate grid density zones. DES model based on Spalart-Allmaras one equation turbulence model which is also called DES97, is used in this thesis.

2.2 Spalart-Allmaras One Equation Model

Spalart-Allmaras one equation model uses the equation (1)

$$\frac{\partial \hat{v}}{\partial t} + u_j \frac{\partial \hat{v}}{\partial x_j} = c_{b1}(1 - f_{t2})\hat{S}\hat{v} - \left[c_{w1} f_w - \frac{c_{b1}}{K^2} f_{t2}\right]\left(\frac{\hat{v}}{d}\right)^2 + \frac{1}{\sigma}\left[\frac{\partial}{\partial_{x_j}}\left((v + \hat{v})\frac{\partial \hat{v}}{\partial_{x_j}}\right)\right.$$

$$\left. + c_{b2}\frac{\partial \hat{v}}{\partial_{x_i}}\frac{\partial \hat{v}}{\partial_{x_i}}\right] \quad (1)$$

And with the equation (2) the turbulent eddy viscosity is calculated:

$$\mu_t = \rho \hat{v} f_{v1} \quad (2)$$

were

$$f_{v1} = \frac{X^3}{X^3 + c^3_{v1}} \quad (3)$$

$$X = \frac{\hat{v}}{v} \quad (4)$$

and ρ is the density, $v = \mu/\rho$ is the molecular kinematic viscosity, and μ is the molecular dynamic viscosity. The additional definition is expressed by the following formula.

$$\hat{S} = \Omega + \frac{\hat{v}}{K^2 d^2} f_{v2} \quad (5)$$

Where $\Omega = \sqrt{2W_{ij}W_{ij}}$ is the magnitude of the vorticity, *d* is the distance from the field point to the nearest wall, and

$$f_{v2} = 1 - \frac{X}{1 + X f_{v1}} \qquad f_w = g\left[\frac{1 + c^6_{w3}}{g^6 + c^6_{w3}}\right]^{1/6} \quad (6)$$

$$g = r + c_{w2}(r^6 - r) \quad (7)$$

$$r = \min\left[\frac{\hat{v}}{\hat{S}K^2 d^2}, 10\right] \quad (8)$$

$$f_{t2} = c_{t3}\exp\left(-c_{t4}X^2\right) \quad (9)$$

$$W_{ij} = \frac{1}{2}\left(\frac{\partial u_i}{\partial x_j} - \frac{\partial u_j}{\partial x_i}\right) \quad (10)$$

the boundary conditions are:

$$\hat{v}_{wall} = 0 \qquad \hat{v}_{farfield} = 3v_\infty : to : 5v_\infty \quad (11)$$

Note that these boundary conditions for the SA turbulent field variable correspond to the following turbulent flow viscosity values:

$$\hat{v}_{t,wall} = 0 \qquad \widehat{vt}_{,farfield} = 0.210438v_\infty : to : 1.294234v_\infty \quad (12)$$

The constants are:

$c_{b1} = 0.1355$ $\sigma = 2/3$ $c_{b2} = 0.622$ $\mathrm{K} = 0.41$

$c_{w2} = 0.3$ $c_{w3} = 2$ $c_{v1} = 7.1$ $c_{t3} = 1.2$

$c_{t4} = 0.5$

$$c_{w1} = \frac{c_{b1}}{\mathrm{K}^2} + \frac{1+c_{b2}}{\sigma} \quad (13)$$

2.3 Spalart-Allmaras based DES model

The one equation SA model solves modified eddy viscosity $\tilde{v}$. To obtain SA version of DES 'd' (turbulence distance scale) is changed with

$$d_{DES} = \min(d, C_{DES}\Delta). \quad (14)$$

d_{DES} is the DES distance scale, C_{DES}=0.65 and Δ is the local grid distance in the domain.

Δ is greater than d in the solid boundaries due to the standard SA model remain unchanged to predict flow RANS model is used. At the regions where Δ is less than 'd' (the regions away from the solid boundaries) equation changes to $\tilde{\nu} \sim S\Delta^2$ where S is the absolute vorticity. So Smagorinsky eddy viscosity is seen then LES model is operated. (Budak,2017)

2.4 Main Parameters, Computational Domain and Mesh Generation

In this study two cases are simulated. Also, a comparison was done between Case I and Kirkil and Constantinescu (2015)'s numerical study which is conducted on flat bed conditions at a comparable Reynolds number with Case I. In simulations, channel and pier dimensions are same however flow conditions are different from the view of Reynolds number. In the first case Reynolds number is 52480, While in the second case it is 262400. In simulations, inclined bed condition is examined; on the other hand, comparison study of the Kirkil and Constantinescu (2015)'s numerical study was conducted on the flatbed conditions In the simulations all dimensions are non-dimensionalized by the pier diameter D. The channel is 30D long and 7.5D wide. The bridge pier was placed at a distance of 10D from the entrance section. The depth of the channel varies between 0.25D and 2.375D. Dimensions used in simulations are shown in figure 2.2.

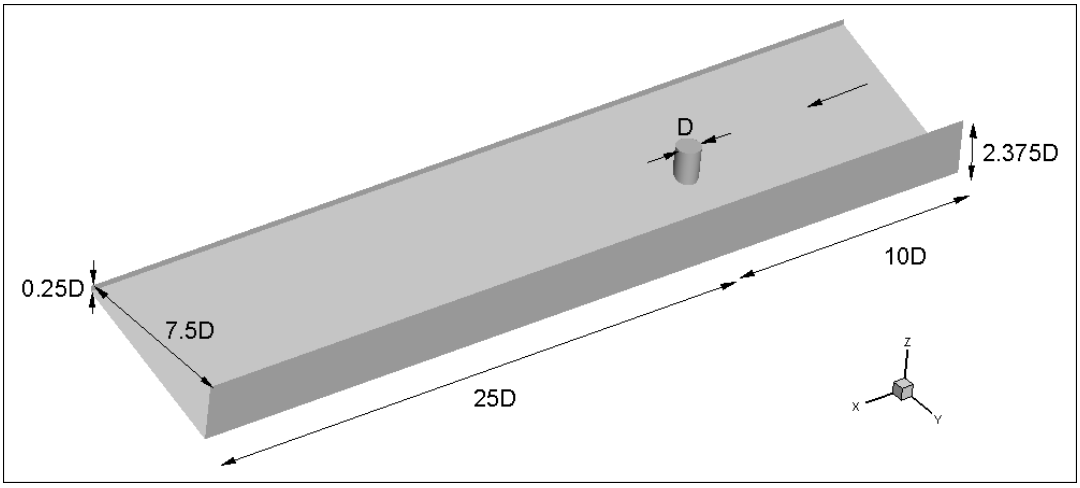

Figure 2.2: General view of study area

In order to get numerical solution, the domain of the selected test case must be meshed by mesh generators. Pointwise software is used to generate meshed domain. Rectangular and structured grids are used in all simulations. Because structured grids have high degree of quality & control, have better alignment thus better convergence, require less memory and time. For structured mesh, the design also covers the data for geometrically similar elements for memory. As a result, fewer cache misses mean

more structured data is used in memory bandwidth. This allows you to use solution algorithms that are not applicable to unstructured data. Boundary conditions and turbulence model implementations work well when functions such as walls and wakes have well-defined numeric paths. The transverse normal are easily identifiable in a standardized grid.

Generation of grids is one of the most important steps in this thesis like all works with meshes. DES turbulence model has a specific grid type that named as DES grid. As Spalart elucidated in "Young-Person's Guide Simulation Grids" (Spalart, 2011) there are important points of gridding in both RANS and LES regions.

RANS region which is efficient at boundaries, near walls entails fine mesh and high aspect ratio due to boundary layer treatment and to reduce number of the cells respectively y+ value should be around 1. Also, increment of cell sizes should not be higher than 1.15. With the intention of estimating the first layer thickness in the geometries Equation 15 given below is used. In this equation, first layer thickness is a function of Reynold number.

$$y^+ = \frac{y * u_*}{\upsilon} \tag{15}$$

where y is the non-dimensional first layer thickness. On the contrary to RANS region LES region is efficient at the rest of the domain. At this region cell sizes can be increased in reasonable manner.

All dimensions were normalized with the pier diameter D=16 cm. Then minimum mesh size calculated as following.

$$Re = \frac{Vh}{\upsilon} = \frac{0.328 * 0.16}{1 * 10^{-6}} = 52480$$

$$y^+ = \frac{y * u_*}{\upsilon}$$

$$\frac{u_*}{V} \cong 0.04$$

$$u_* = 0.328 * 0.04 = 0.01312\ m/s$$

$1 = y * 0.01312 * 52480$

$y = 0.00145\ m$

$y/D \cong 0.009$

While creating mesh around pier and side walls minimum nondimensional mesh size 0.009 and 4.4 million total mesh were used for case I. For Case II Reynold's Number exact 5 times of the Reynold's Number at Case I. Minimum mesh size at Case II is one fifth of the minimum mesh size at the Case I. Thus, minimum mesh size at Case II y=0.0018 and 6.1 million total mesh were used for case II. Using minimum mesh size around these locations is quite significant resolve the boundary layer correctly. Between these locations mesh sizes increased smoothly. (Figure 2.3)

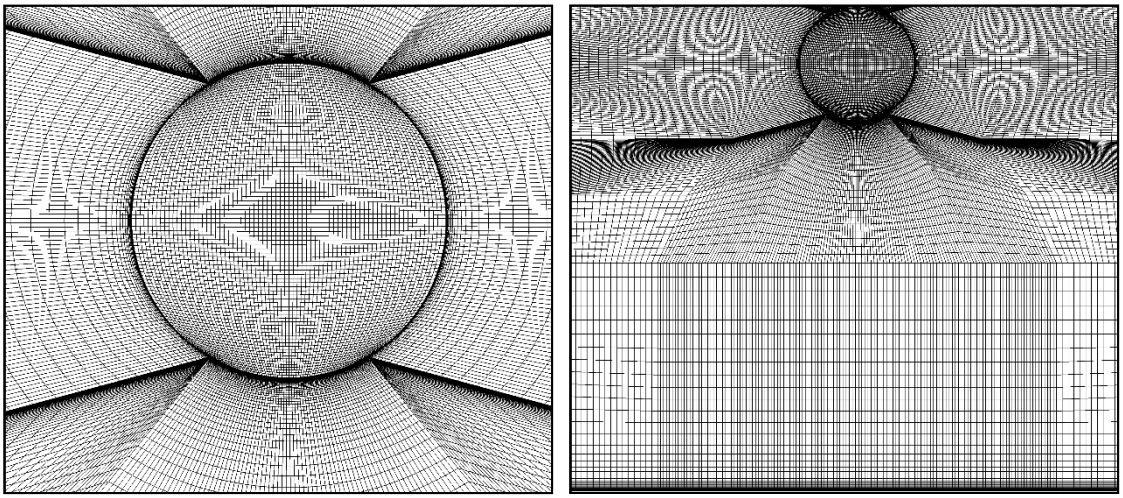

Figure 2.3: A view from the mesh around pier and between pier and the walls

During the computations RANS-LES hybrid model (DES) was used. After the mesh is created it is divided into 16 partitions which is run parallel on TRGRID on 16 processors. Initially, a RANS solution is achieved which was necessary as an initial condition for the DES simulations. Once it is converged DES is started. Same process was applied to both Case I and Case II.

In the numerical part of the study, Spalart-Allmaras DES model deprived of wall functions is applied. A completely implicit fractional step method is used to integrate the incompressible 3D Navier-Stokes equations. The convection term from the

momentum equation is discretized by a mixture of the exact fifth-order upwind bias scheme and the central quadratic scheme, with the aim of lowering the level of numerical dissipation. (Köken, 2017)

In simulations wall functions were not used and viscous sublayer was solved directly. For this purpose, the meshes was denser in the areas close to the wall and the first point of mesh created was positioned as $y^+=1$ ($y^+ = yu*/v$).

2.5 Validation

The code executed in this study is validated the various flow conditions associated with the flow around the pier. (Constantinescu, Koken, & Zeng, 2011; Kirkil & Constantinescu, 2010). Experimental and numerical results were consistent with each other. The code executed in this study has also been validated with detailed experimental data for various flow conditions. (Chang, Constantinescu, & Park, 2007; Constantinescu, Koken, & Zeng, 2011; Constantinescu & Squires, 2004; Koken, 2011). In addition, grid generation method validated in these studies. Thus, a grid dependence study was not done in the scope of this thesis.

2.6 Boundary and Initial Conditions

At the inflow section, a velocity profile was used as boundary condition. This profile was obtained from another simulation conducted on same sized but pier - free channel. Then a synthetic turbulence profile added to the flow profile. (Demirbaş, 2021).

At the rigid surfaces, no-slip boundary condition was used, which means that velocity of the fluid is zero at the boundary and water surface was assumed as a rigid surface. This assumption is acceptable because Froude number in the simulations is low. (0.4) (Budak,2017)

At the outlet section, vortices are consented to leave the domain without triggering any unphysical oscillations.

CHAPTER 3

RESULTS AND DISCUSSION

3.1 Effect of Reynolds Number

In this chapter obtained results for Case I and Case II are compared.

The model dimensions and the three cross-sections on the canal are shown Figure 3.1. The Isolated pier is located at 10D downstream of the inlet section whereas a total length of 35D of the channel is modelled in the study. Turbulent kinetic energy and velocity values at three cross-sections are investigated which were given in Figure 3.1. These cross-sections that are labelled as a, b, c are taken at x=10D, 15D and 25D from the inlet section, respectively.

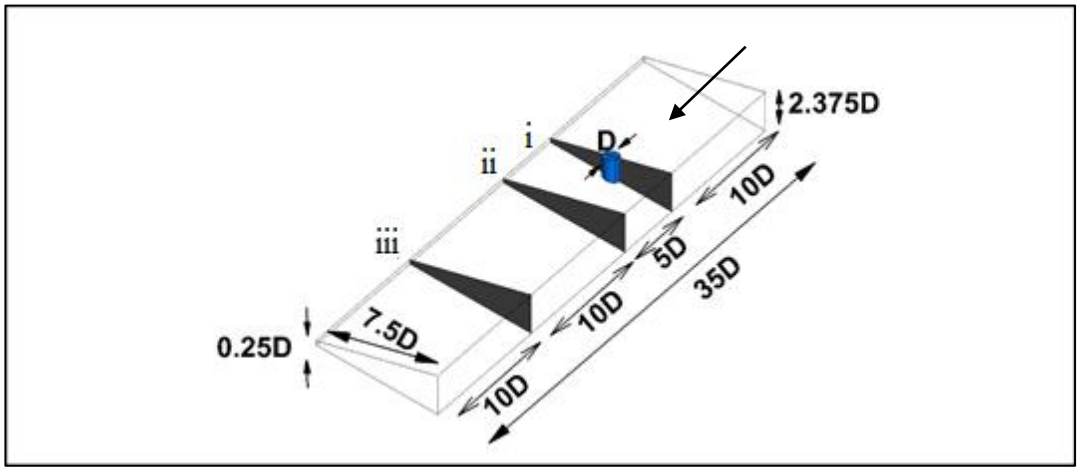

Figure 3.1 Flow domain and the cross-sections used in the study

3.1.1 Velocity and Vorticity Distribution for the Mean Flow

Non-dimensional streamwise velocity magnitude at vertical sections (i),(ii), and (iii) are given for Case-I in Figure 3.2. At the pier section large velocity magnitudes are observed on both sides of the pier. However, at further downstream, velocity values are larger on the deep side of the channel.

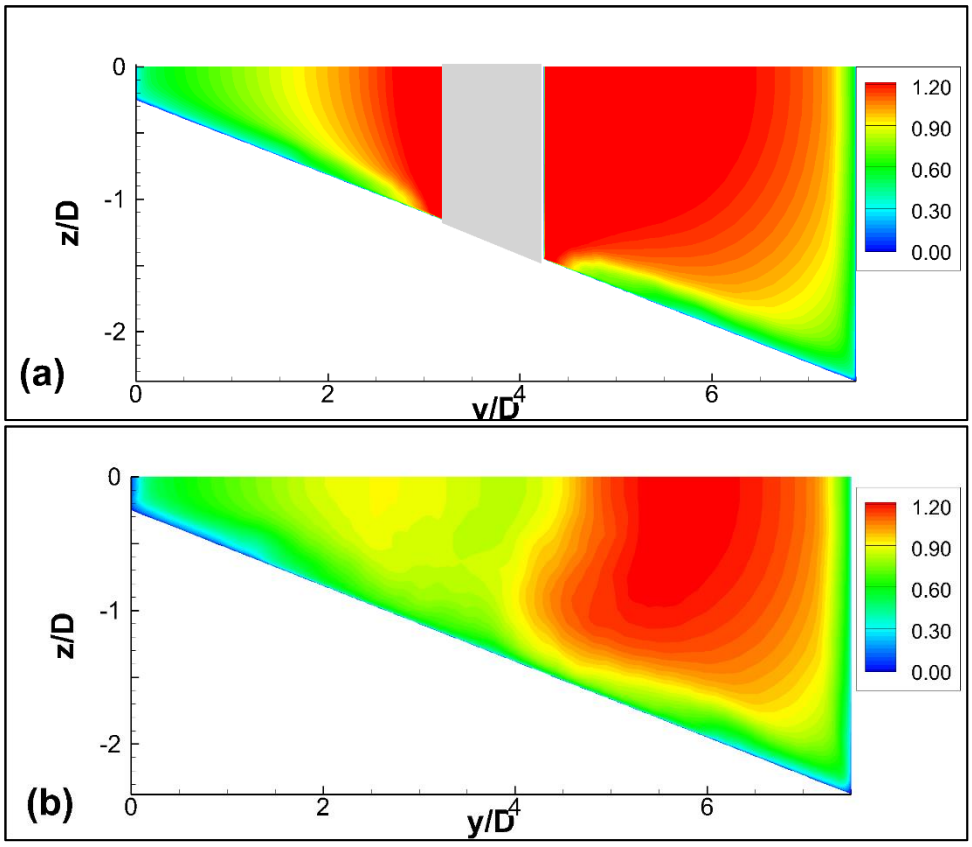

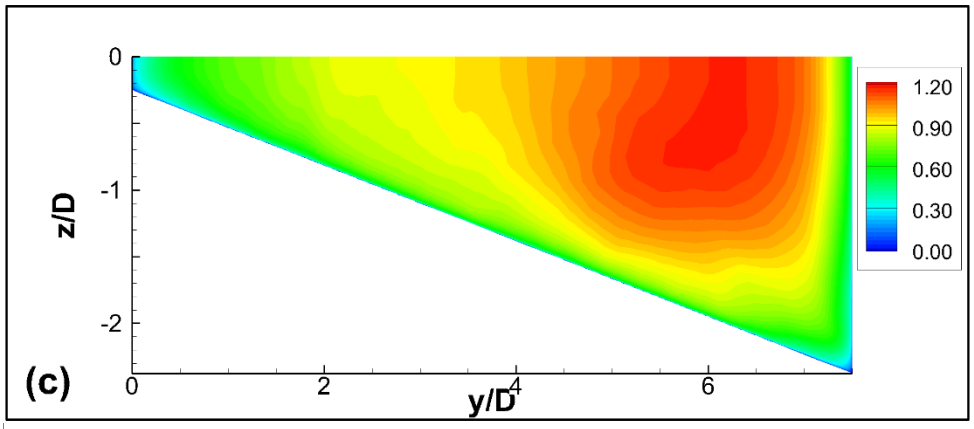

Figure 3.2 Non-dimensional streamwise velocity magnitude u/U at sections a) (i), b) (ii) and c) (iii)

Similar observations are made for Case II.

Nondimensionalized streamwise velocity values on the free surface and at the mid-flow depth for Case I and Case II simulations are given in Figure 3.3 and Figure 3.4, respectively. In both simulations, velocity values along the deep side of the channel are considerably higher compared to the shallow side of the channel. Accelerating flow regions on the shallow side of the channel were observed only in a limited area near the pier. Behind the pier is a recirculation zone where negative velocities are observed. When the velocities in the water-free surface and mid-flow depth are compared, it is seen that the velocities on the free surface are slightly higher. When the simulation Case I and Case II are compared, it has been observed that the maximum dimensionless velocity magnitudes observed in Case II are approximately 3% higher than the values observed in Case I.

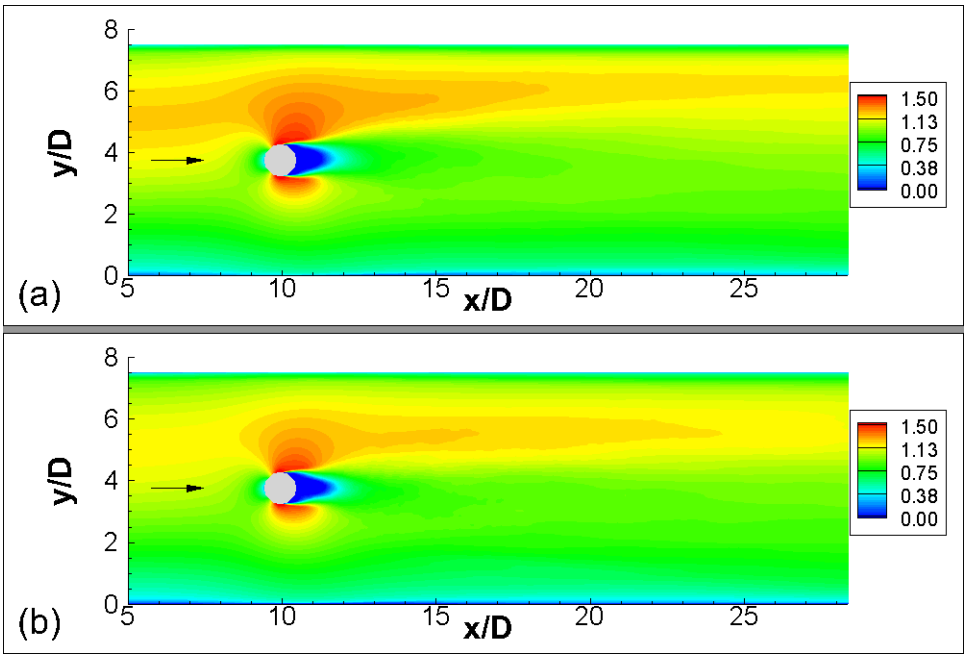

Figure 3.3 Dimensionless Velocity u/U values at average flow conditions for z axis for Case I simulations a) On the free surface of water; b) Water medium depth.

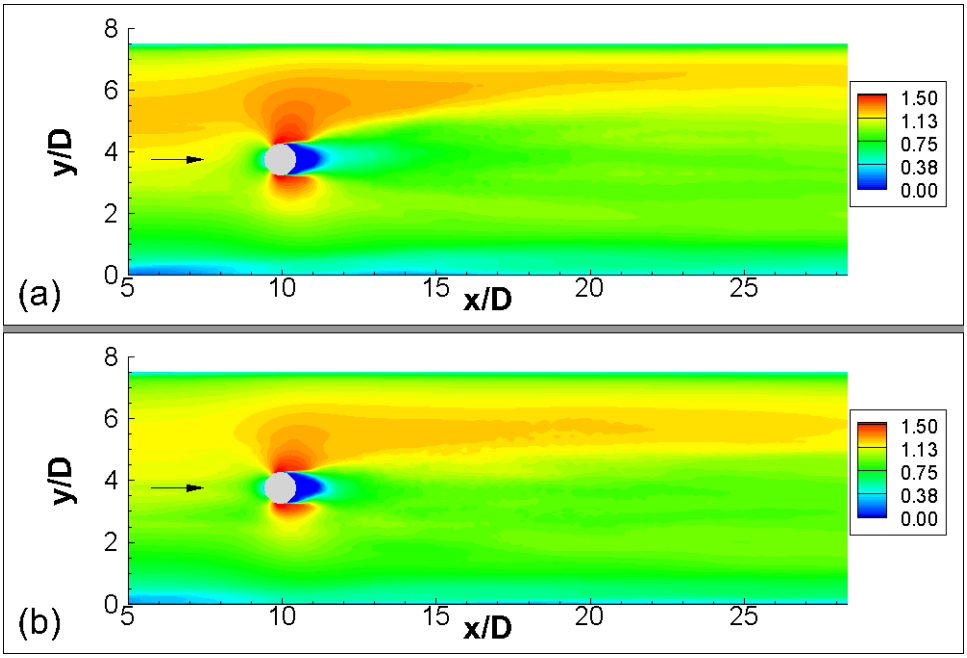

Figure 3.4 Dimensionless Velocity u/U values at average flow conditions for z axis for Case II simulations a) On the free surface of water; b) Water medium depth

In Case I simulation, the separation zones formed behind the bridge pier can be easily distinguished from the dimensionless vertical vortex distributions given in Figure 3.5. The vertical vorticity values in the detached shear layers are considerably larger than the other flow regions. From the shear layers detached in the free surface of the water, the left one (blue zone in Figure 3.5-a) is in a slight orientation towards the deep channel edge (shown by dashed lines in the figure). This orientation disappears when the mid-depth is reached in the canal (Figure 3.5-b). A similar situation was observed in the Case II simulation.

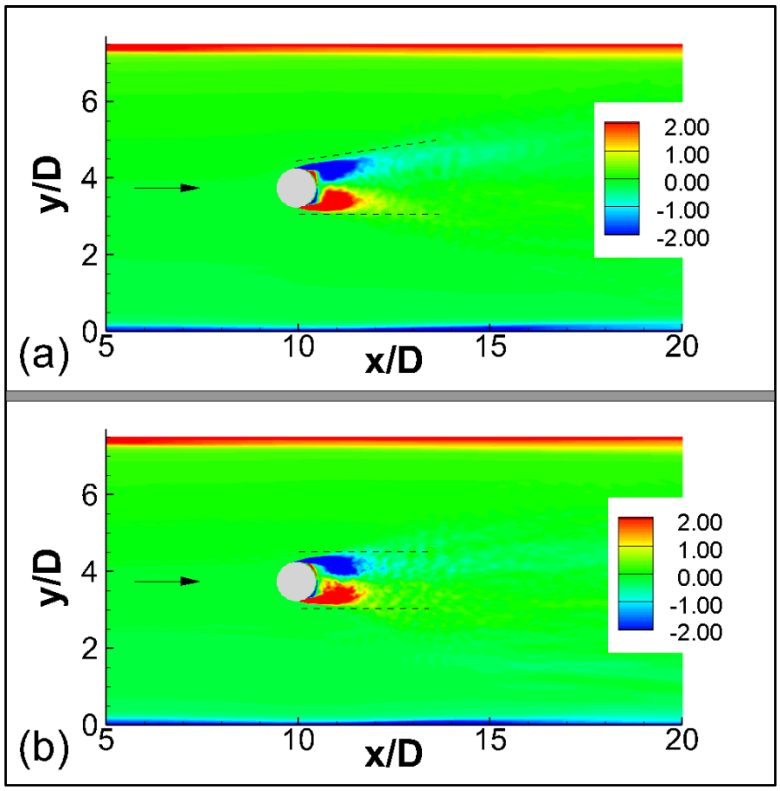

Figure 3.5 Dimensionless vertical vortex distribution at average flow conditions for Case I simulation, $\omega_z D/U$: a) On the free surface of the water; b) Water medium depth.

3.1.2 Turbulent Kinetic Energy Distribution

Dimensionless turbulent kinetic energy distribution in different vertical sections along the axis of the channel is given in Figures 3.6 and 3.7, respectively, for Case I and Case II simulations. In both simulations, turbulent kinetic energy values are very close to each other. In both simulations, it is seen that the turbulent kinetic energy values increase in the vortex downstream of the bridge pier. (Figures 3.6b and 3.7b), and then these values decrease when moving downstream through the channel (Figures 3.6c and 3.7c). In Case I simulation, a noticeable increase in turbulent kinetic energy values is observed on both sides of the bridge pier in the region close to the base in the section taken from the center of the bridge pier. The aforementioned increase is due to the horseshoe vortex in this section. When the Case I and Case II simulations are compared, the lateral propagation of the region with high turbulent kinetic energy in the x / D = 15 section where the turbulent kinetic energy is the densest in the bridge pier is in the range of 2.75 <y / D <5.25 in the Case II simulation, while it is in the range of 3.25 <y / D <5 and it is narrower in the Case I simulation.

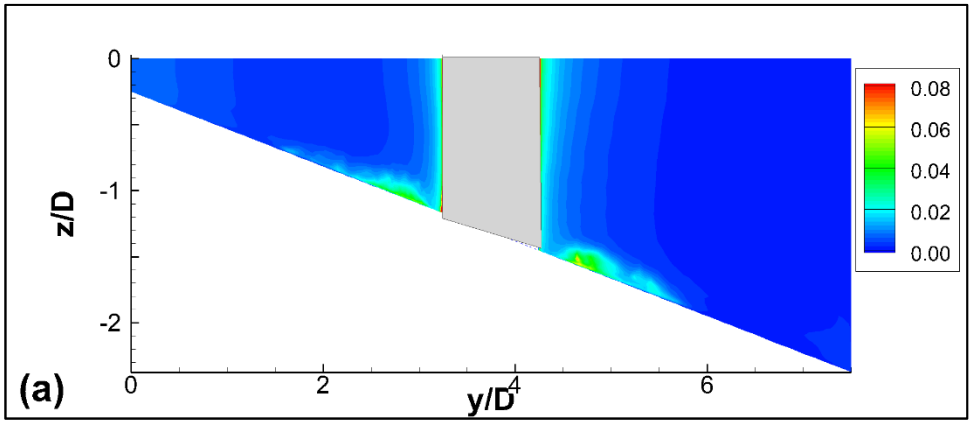

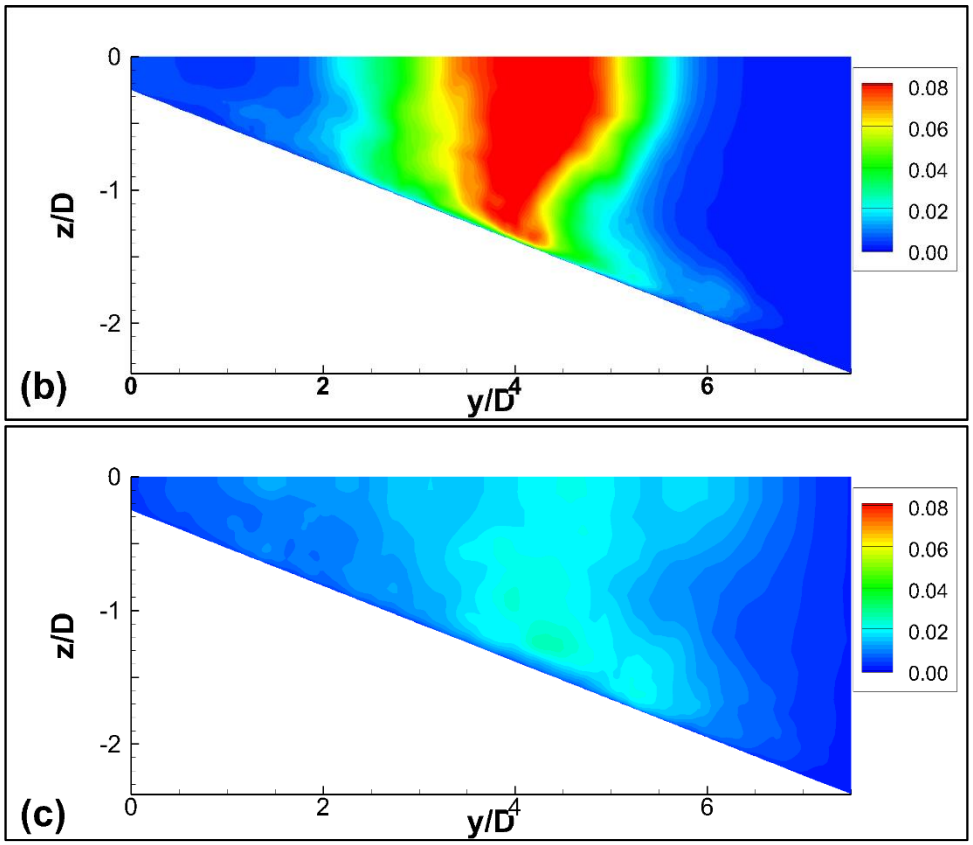

Figure 3.6 Dimensionless turbulent kinetic energy, k/U2, distribution obtained in different vertical sections under average flow conditions for Case I simulation: a) x / D = 10; b) x / D = 15; c) x / D = 25.

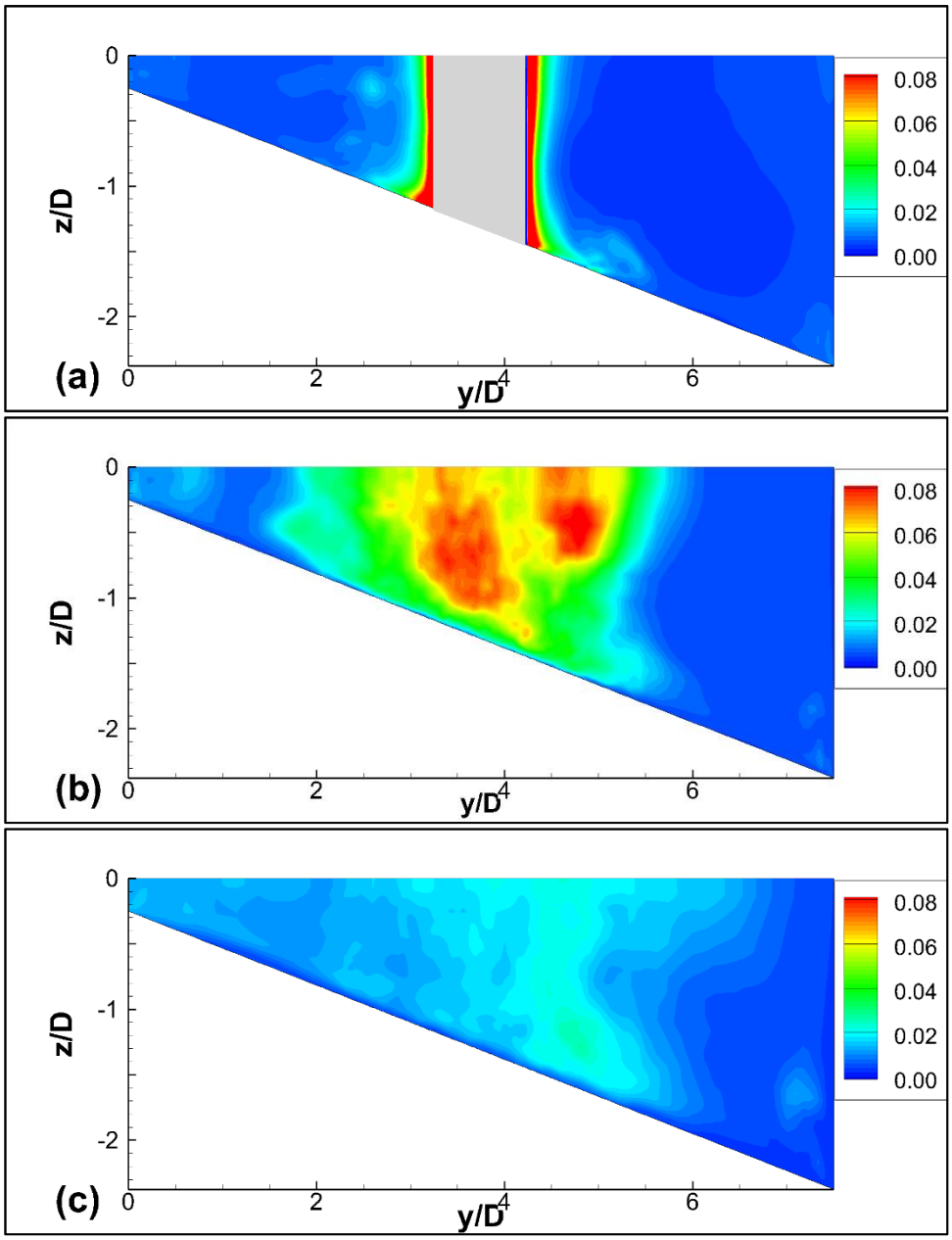

Figure 3.7 Dimensionless turbulent kinetic energy, k/U2, distribution obtained in different vertical sections under average flow conditions for Case II simulation: a) x / D = 10; b) x / D = 15; c) x / D = 25

Nondimensionalized turbulent kinetic energy values on the free surface and at the mid-flow depth for Case I and Case II simulations are given in Figure 3.8 and Figure 3.9, respectively. To compare the simulations made at low and large Reynolds

numbers, it was observed that the region with high turbulent kinetic energy formed behind the bridge pier was approximately 40% wider in the lateral direction in the high Reynolds number solution.

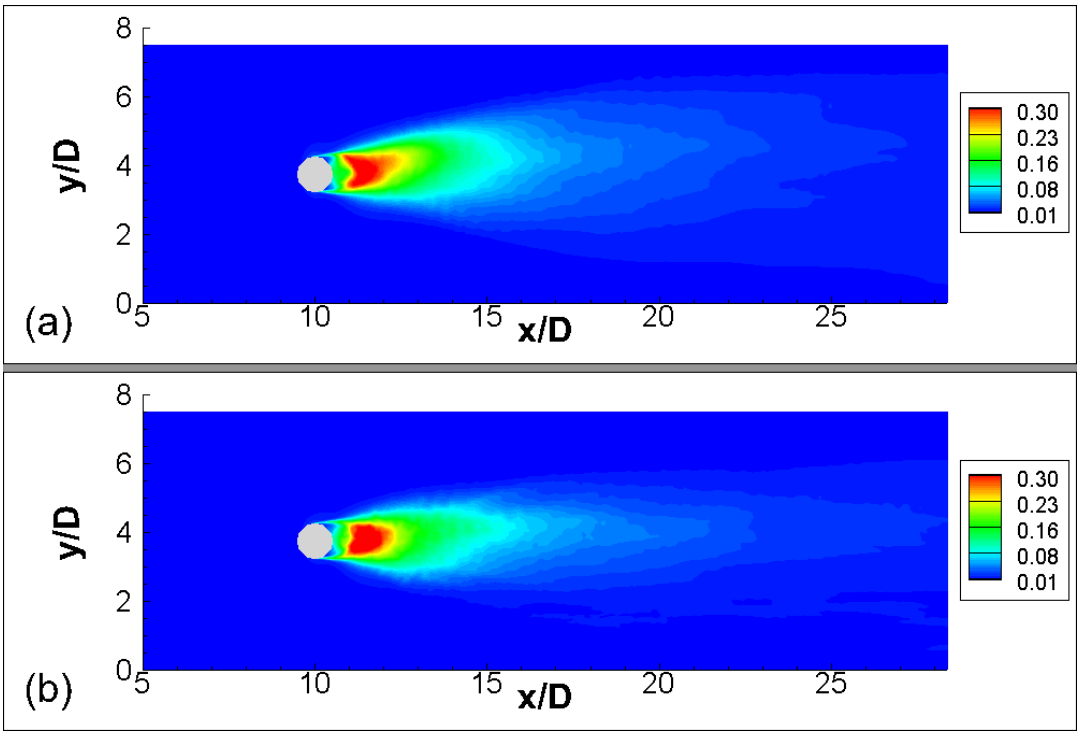

Figure 3.8 Dimensionless turbulent kinetic energy, k/U2, distribution obtained in different horizontal sections under average flow conditions for Case I simulation: a) On the free surface of the water; b) Water medium depth.

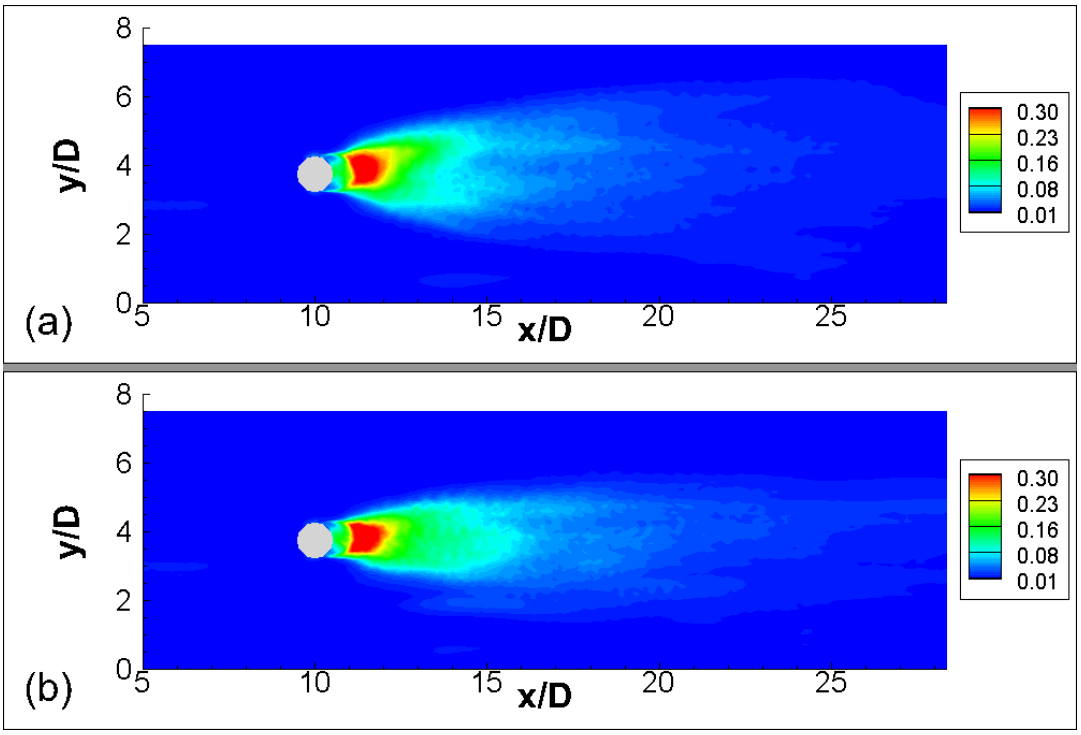

Figure 3.9 Dimensionless turbulent kinetic energy, k/U2, distribution obtained in different horizontal sections under average flow conditions for Case II simulation a) On the free surface of the water; b) Water medium depth.

3.1.3 Coherent Structures Around the Piers

The flow structures around the pier in Case I and Case II simulations (Dubief & Delcayre, 2000) was showed in 3D for the average flow with using Q-criterion. The Q-criterion is one of the most benefitted techniques to envisage the coherent structures for the mean flow. The Q criterion is the number that picture the vortical structures and it is the second constant of the velocity gradient tensor ($Q = -0.5(\frac{\partial u_i}{\partial u_j} x \frac{\partial u_j}{\partial u_i})$ (Constantinescu et al., 2011)

Figure 3.10 shows that in both simulations, at the upstream side of the bridge pier, close to the base, the horseshoe vortexes surrounding the pier from both sides were observed. Apart from this, two wake vortexes with vertical axes were observed at the downstream of the pier. In Case I simulation, the horseshoe vortex is asymmetrical and stronger on the deep side of the channel, while the horseshoe

vortex is symmetrical in the Case II simulation. Comparing the Case I and Case II simulations, the horseshoe vortex is longer in Case II than in Case I.

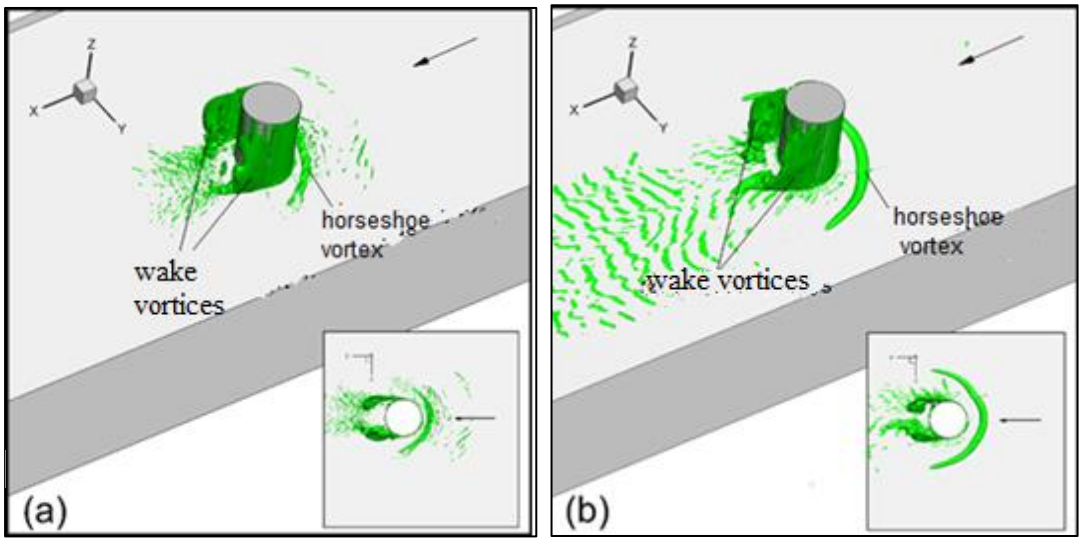

Figure 3.10 Representation of coherent structures forming around pier using Q-criterion for: a) Case I b) Case II

While the horseshoe vortex is strongest at the upstream part of the pier, it loses its strength as it moves downstream. Dimensionless vorticity magnitude and dimensionless turbulent kinetic energy distributions in vertical (i) and (ii) sections (see Figure 3.11) are given in Figure 3.12. In this figure, the white arrow indicates the position of the horseshoe vortex. As can be seen here, the vortex and turbulent kinetic energy values increase in the center of the horseshoe vortex. When progressed towards to the downstream, effect of the horseshoe vortex decreases. In Case I simulation, the horseshoe vortex is formed at a distance of approximately 0.25D from the bridge pier, while this distance is approximately 0.45D in Case II simulation.

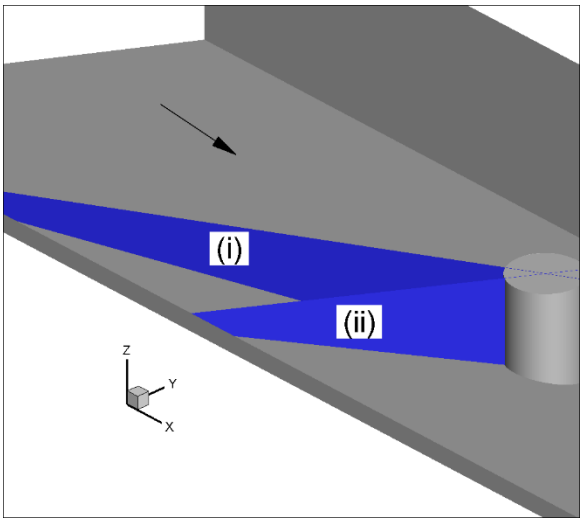

Figure 3.11 (i) and (ii) sections

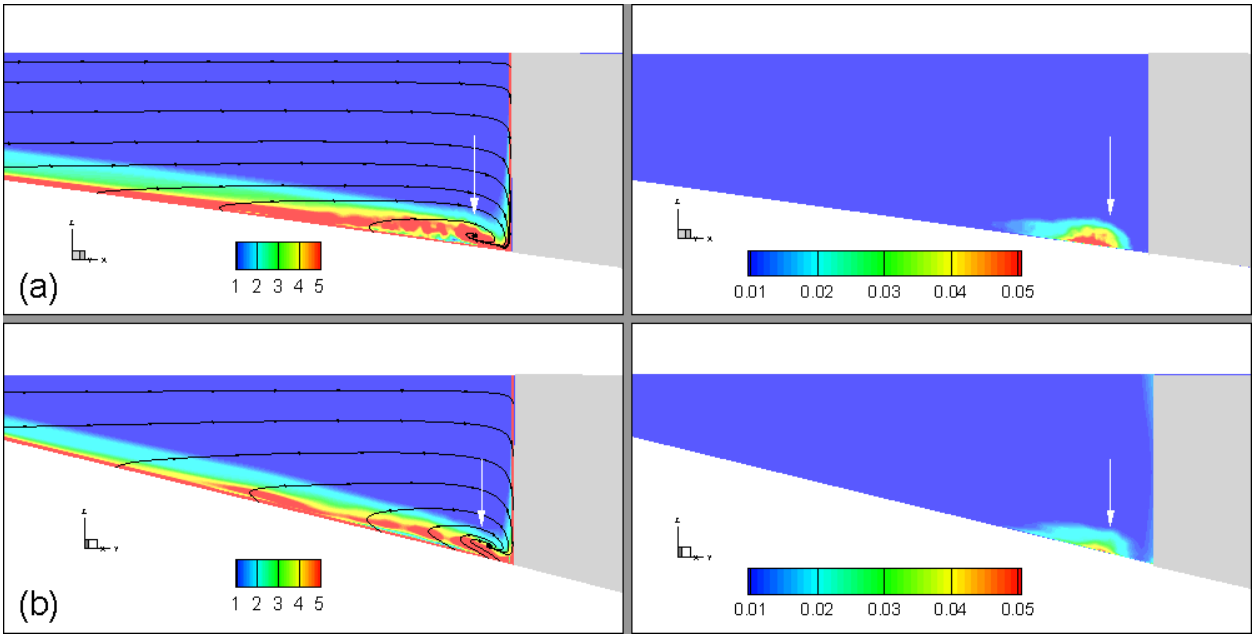

Figure 3.12 In Case I simulation, streamlines and dimensionless vorticity magnitude $\omega_t D/U$ (left) and dimensionless turbulent kinetic energy, k/U2, (right) in a) (i) section; b) In section (ii).

3.1.4 Bed Shear Stress Distribution

Dimensionless bed shear stress values, $\tau_w/(\rho U^2)$, obtained for average current in Case I and Case II simulations are given in Figures 3.13 and 3.14, respectively. In both simulations, the bed shear stress values increase on both sides of the bridge pier, along the axis of the horseshoe vortex and downstream of the pier in the regions where the flow accelerates. While the maximum bed shear stress value in Case I simulation is 0.011, this value is approximately 0.006 in Case II simulation. In both simulations, the region where the bed shear stress values increase is effective in a slightly larger area on the side of the bridge pier where the current is shallow, and the maximum bed shear stress values occur adjacent to the pier in this region.,

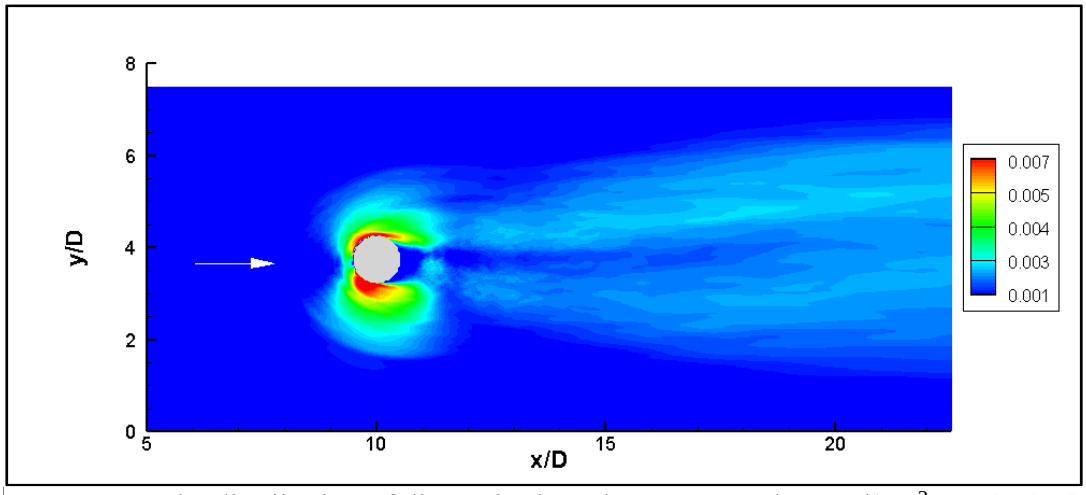

Figure 3.13 The distribution of dimensionless shear stress values $\tau_w/(\rho U^2)$ on the bed at average flow conditions for Case I simulation.

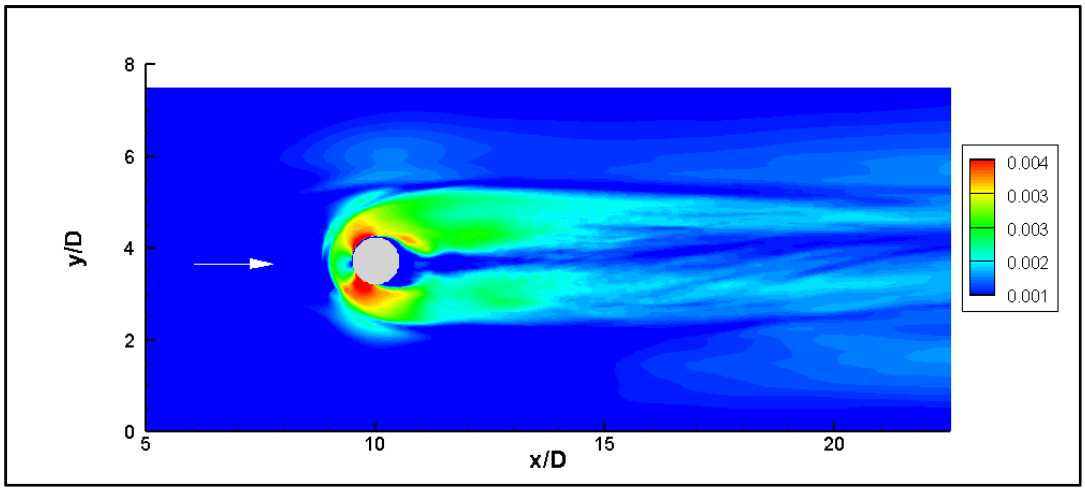

Figure 3.14 The distribution of dimensionless shear stress values $\tau_w/(\rho U^2)$ a
on the bed at average flow conditions for Case II simulation.

3.2 Effect of Bed Inclination

In this chapter obtained results for Case I are compared with Kirkil and Constantinescu's (2015) study named "*Effects of cylinder Reynolds number on the turbulent horseshoe vortex system and near wake of a surface-mounted circular cylinder".* At the researchers' study Reynolds number is $5x10^4$ which is very close to Reynolds number at case I in this study, non- dimensionalized pier diameter is "D" and channel depth is continuous 1.12D.

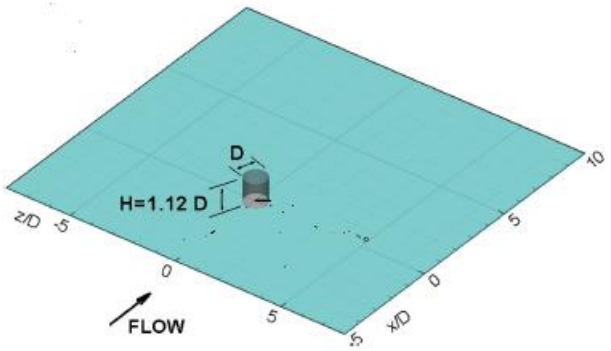

Figure 3.15 General View of the Study Area

3.2.1 Turbulent Kinetic Energy Distribution

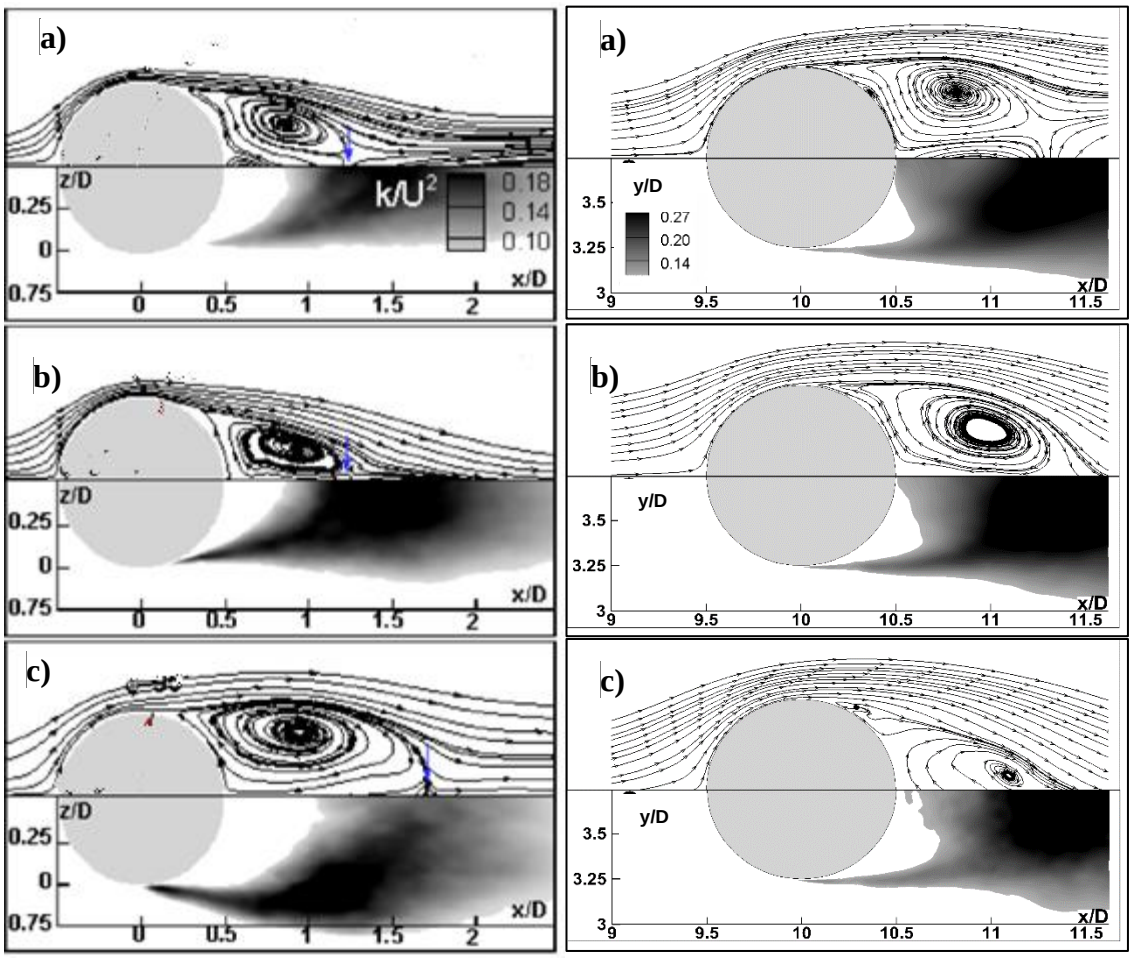

Figure 3.16 Turbulent kinetic energy, k/U^2, and 2-D streamline patterns in horizontal planes for the comparison study of Kirkil and Constantinescu (2015) (left) and Case I (right) at(a) z/D= 1; (b)z/D= 0.5; (c) z/D= 0.1. Values of k/U^2 less than 0.08 were blanked out.

In figure 3.16 streamlines and Turbulent kinetic energy, k/U^2 distribution was shown for Case I and the comparison study of Kirkil and Constantinescu (2015). Figure 3.16 shows that the recirculation zones at the downstream of the cylinder are symmetrical at all depths in the reference study. On the other hand, in Case 1 because of the inclination on the bed, the recirculation zones lose their symmetry and tend to be tilted towards the shallower channel side, at water depths close to the channel bed (See Fig. 3.16 c). It was also observed that turbulent kinetic energy levels in Case I

are approximately 50% higher with respect to the flat bed simulations. One other difference is in the pattern of the high turbulent kinetic energy levels. Inside the wake along the symmetry axis of the cylinders, amplified turbulent kinetic energy levels are observed at approximately 0.75-1D distance from the cylinder surface in the reference study whereas in Case I this amplification starts from the cylinder surface.

3.2.2 Mean Bed Friction Velocity

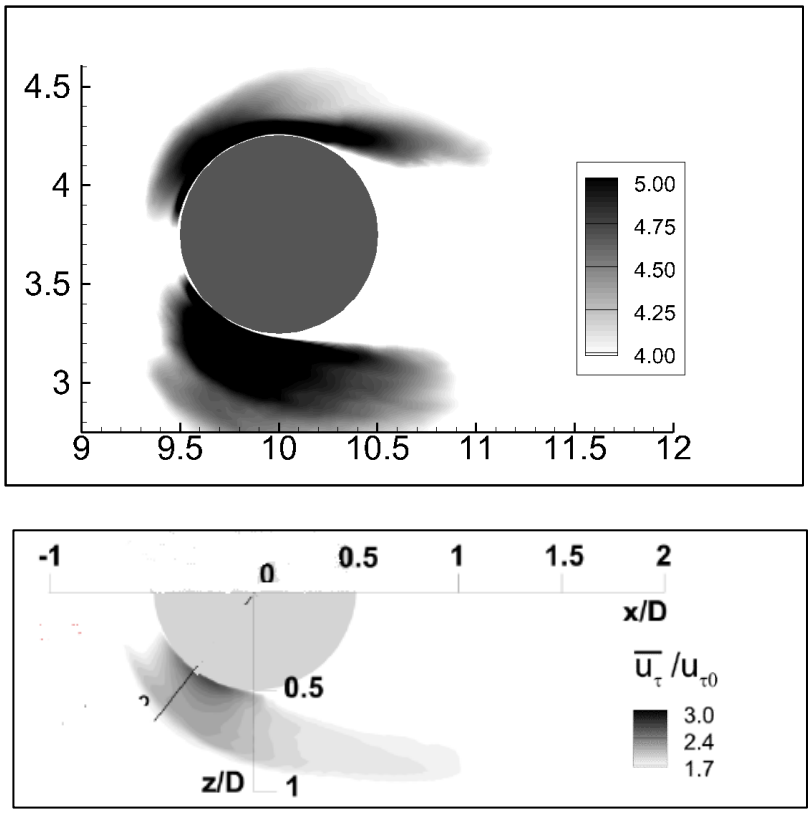

Figure 3.17 Mean bed friction velocity $\overline{u_r}/u_{r0}$ in Case I(top) and in comparison, study of Kirkil and Constantinescu (2015) (bottom)

Figure 3.17 shows the non-dimensional bed friction velocity ratios for the mean flow $\overline{u_r}/u_{r0}$ for Case I and the comparison study. Here u_{r0} is the mean reference bed friction velocity in the incoming fully turbulent flow away from the cylinder. Shear velocity values are amplifed as much as three times in the comparison study whereas

in Case I maximum amplification ratio is more than five. On the deeper channel side of the pier, Case I shows a similar amplification pattern compared to Kirkil and Constantinescu (2015) with larger amplification ratios. This comparison demonstrates that the inclined channels are more critical in terms of the scour risk.

CHAPTER 4

CONCLUSIONS

This thesis implemented Detached Eddy Simulations (DES) investigations of flow and turbulence structure around a bridge pier conducted for conditions typically encountered in large-scale laboratory experiments in Katip Çelebi University with the scope of the TUBITAK 116M519 coded project Scientific and Technological Research Council of Turkey

In this thesis, two scenarios are examined, both of which have flatbed conditions that represent the initiation of the scouring process. These scenarios are based on two separate Reynolds numbers and two different bed conditions. At the first case Reynolds number is 52,480 is typical for flume experiments. At the second case Reynolds number is 262,400 that represents the physical conditions found in nature. In addition, results of Kirkil and Constantinescu's(2015) study named "*Effects of cylinder Reynolds number on the turbulent horseshoe vortex system and near wake of a surface-mounted circular cylinder"* which performed in similar conditions with case I was used and compared with the results of Case I

The turbulent flow structures formed around the bridge pier placed in a triangular section channel and the bed shear stress distribution were investigated using the DES turbulence model in both laboratory conditions (Case I) and flow conditions (Case II) that can be observed in river flows in practice.

In both simulations, it has been observed that the velocities in the channel are greater in the deep part of the flow. In addition, a region where the velocity increases locally is formed on the shallow side of the channel near the bridge pier.

In both cases, it was observed that the horseshoe vortex was formed around the pier and two recirculation zones were formed downstream of the pier under average flow conditions. When the horseshoe vortex moves in the direction of flow, it loses its

coherence. In the simulation made at low Reynolds number, it was seen that the horseshoe vortex formed at a position closer to the bridge pier.

Turbulent kinetic energy values increase along the axis of the horseshoe vortex and downstream of the bridge pier. To compare the simulations made at low and large Reynolds numbers, it was observed that the region with high turbulent kinetic energy formed behind the bridge pier was approximately 40% wider in the lateral direction in the high Reynolds number solution.

From the detached shear layers formed on both sides of the bridge pier, the one at the deep side shows orientation towards the side wall of the bridge in the region close to the water surface. This orientation disappears at medium depth and occurs in the direction of the current.

When the bed shear stress distribution formed on the base is examined, it is observed that high soil stress values occur in the acceleration regions on both sides of the bridge pier and along the detached shear layers. In both simulations, these stresses are observed to be effective across a wider band on the shallow canal side than on the deep canal side. Maximum bed shear stress values also occurred on this shallow side. While the maximum dimensionless bed shear stress value is 0.011 in the low Reynolds number simulation, this value is 0.006 in the high Reynolds number simulation.

Compared to Kirkil and Constantinescu (2015)'s numerical study which is conducted on flat bed conditions at a comparable Reynolds number with Case I; it was observed that amplification in shear velocity values around the pier are much larger in the inclined channel case. This means that inclined channels are exposed to scour more compared to the flat bed channels.

REFERENCES

Aghaee, Y., & Hakimzadeh, H. (2010). Three-dimensional numerical modeling of flow around bridge piers using LES and RANS.

Bouabdellah, G. (2019). REDUCTION OF SCOUR AROUND BRIDGE PIERS USING A VORTEX GENERATOR. Journal Of Flow Visualization and Image Processing, 26(3), 279-299. doi: 10.1615/jflowvisimageproc.2019029301

Breuer, M. (1998). Large eddy simulation of the subcritical flow past a circular cylinder: numerical and modeling aspects. *International Journal for Numerical Methods in Fluids*, *28*(9), 1281–1302.

Budak E. (2017) "Numerical Investigatıon of Flow Around an Isolated Spur Dıke in a Curved Channel".", Master Thesis, Middle East Technical University, Ankara.

Chang, K., Constantinescu, G., & Park, S. (2007). Assessment of Predictive Capabilities of Detached Eddy Simulation to Simulate Flow and Mass Transport Past Open Cavities. *Journal Of Fluids Engineering*, *129*(11), 1372-1383. doi: 10.1115/1.2786529

Cheng, Z., Koken, M., & Constantinescu, G. (2018). Approximate methodology to account for effects of coherent structures on sediment entrainment in RANS simulations with a movable bed and applications to pier scour. *Advances In Water Resources*, *120*, 65-82. doi: 10.1016/j.advwatres.2017.05.019

Constantinescu, G., & Squires, K. (2004). Numerical investigations of flow over a sphere in the subcritical and supercritical regimes. *Physics Of Fluids*, *16*(5), 1449-1466. doi: 10.1063/1.1688325

Constantinescu, G., Koken, M., & Zeng, J. (2011). The structure of turbulent flow in an open channel bend of strong curvature with deformed bed: Insight provided by detached eddy simulation. *Water Resources Research*, *47*(5). doi: 10.1029/2010wr010114

Constantinescu, G., Koken, M., & Zeng, J. (2011). The structure of turbulent flow in an open channel bend of strong curvature with deformed bed: Insight provided by detached eddy simulation. *Water Resources Research*, *47*(5). doi: 10.1029/2010wr010114

Cui, W., Zhang, X., Li, Z., Li, H., & Liu, Y. (2017). Three-dimensional numerical simulation of flow around combined pier based on detached eddy simulation at high Reynolds numbers. *International Journal Of Heat And Technology*, *35*(1), 91-96. doi: 10.18280/ijht.350112

Demirbaş, G. D. (2021). "Numerıcal investigation of wind load characteristics around an isolated tall building.", Master Thesis, Middle East Technical University, Ankara.

Ercan, E., & Gündoğan, G. (2012, April 7). 61 yıllık köprü çöktü... Araçlar içindekilerle birlikte suya gömüldü... 15 kişi kayıp... Retrieved July 17, 2020, from https://www.hurriyet.com.tr/gundem/61-yillik-kopru-coktu-araclar-icindekilerle-birlikte-suya-gomuldu-15-kisi-kayip-20290763

Flint, M., Fringer, O., Billington, S., Freyberg, D., & Diffenbaugh, N. (2017). Historical Analysis of Hydraulic Bridge Collapses in the Continental United States. *Journal Of Infrastructure Systems*, *23*(3), 04017005. doi: 10.1061/(asce)is.1943-555x.0000354

Ghenim, A., Seddini, A., & Guemou, B. (2016). Numerical investigations of the round-nosed bridge pier length effects on the bed shear stress. *Progress In Computational Fluid Dynamics, An International Journal*, *16*(5), 313. doi: 10.1504/pcfd.2016.10000218

Girimaji, S. S. (2005). Partially-Averaged Navier-Stokes Model for Turbulence: A Reynolds-Averaged Navier-Stokes to Direct Numerical Simulation Bridging Method. *Journal of Applied Mechanics, 73*(3), 413-421. doi:10.1115/1.2151207

Guemou, B., Seddini, A., & Ghenim, A. (2018). Scour around Bridge Piers: Numerical Investigations of the Longitudinal Biconcave Pier

Shape. *Periodica Polytechnica Mechanical Engineering*, *62*(4), 298-304. doi: 10.3311/ppme.12263

Harik, I., Shaaban, A., Gesund, H., Valli, G., & Wang, S. (1990). United States Bridge Failures, 1951–1988. *Journal Of Performance of Constructed Facilities*, *4*(4), 272-277. doi: 10.1061/(asce)0887-3828(1990)4:4(272)

Hoffmann, K. A., & Chiang, S. T. (n.d.). *Volume 3*. Wichita, KS: Engineering Education System. USA, August 2000.

Kirkil, G., & Constantinescu, G. (2015). Effects of cylinder Reynolds number on the turbulent horseshoe vortex system and near wake of a surface-mounted circular cylinder. *Physics of Fluids*, *27*(7), 075102. https://doi.org/10.1063/1.4923063

Kirkil, G., Constantinescu, G., & Ettema, R. (2009). Detached Eddy Simulation Investigation of Turbulence at a Circular Pier with Scour Hole. *Journal Of Hydraulic Engineering*, *135*(11), 888-901. doi: 10.1061/(asce)hy.1943-7900.0000101

Koken, M., & Constantinescu, G. (2009). An investigation of the dynamics of coherent structures in a turbulent channel flow with a vertical sidewall obstruction. *Physics Of Fluids*, *21*(8), 085104. doi: 10.1063/1.3207859

Li, J., Tao, J., & Liu, Y. (2017). DES Modeling of Erosional Forces around Streamlined Piers and Implications for Scour Countermeasures. International Journal of Geomechanics, 17(6), 04016139. doi: 10.1061/(asce)gm.1943-5622.0000839

McCoy, A., Constantinescu, G., & Weber, L. (2007). A numerical investigation of coherent structures and mass exchange processes in channel flow with two lateral submerged groynes. *Water Resources Research*, *43*(5). doi: 10.1029/2006wr005267

McCoy, A., Constantinescu, G., & Weber, L. (2008). Numerical Investigation of Flow Hydrodynamics in a Channel with a Series of Groynes. *Journal Of*

Hydraulic Engineering, *134*(2), 157-172. doi: 10.1061/(asce)0733-9429(2008)134:2(157)

Nishino, T., Roberts, G., & Zhang, X. (2008). Unsteady RANS and detached-eddy simulations of flow around a circular cylinder in ground effect. *Journal of Fluids and Structures*, *24*(1), 18–33. https://doi.org/10.1016/j.jfluidstructs.2007.06.002

Paciorri, R., Dieudonne, W., Degrez, G., Charbonnier, J., & Deconinck, H. (1997). Validation of the Spalart-Allmaras turbulence model for application in hypersonic flows. *28th Fluid Dynamics Conference*. doi:10.2514/6.1997-2023

Pope, S. B. (2019). *Turbulent flows*. Cambridge: Cambridge University Press.

Soydan, N., Şimşek, O., & Aköz, M. (2016). Eşik Mansabındaki Kritik Üstü Açık Kanal Akımının Deneysel ve Sayısal Analizi. *Çukurova Üniversitesi Mühendislik Mimarlık Fakültesi Dergisi, 31*(2), 33-45.

Spalart, P. R. (2009). Detached-Eddy Simulation. *Annual Review of Fluid Mechanics*, *41*(1), 181-202. doi:10.1146/annurev.fluid.010908.165130

Spalart, P. R. (2011). Young-Person's Guide Simulation Grids.

Travin, A., Shur, M., Strelets, M., & Spalart, P. (2000). etached-Eddy Simulations Past a Circular Cylinder. *Flow, Turbulence and Combustion*, *63*(1/4), 293–313. https://doi.org/10.1023/a:100990140118

Travin, A., Shur, M., Strelets, M., & Spalart, P. (2000). *Flow, Turbulence and Combustion, 63*(1/4), 293-313. doi:10.1023/a:1009901401183

Wilcox, D. C. (2010). *Turbulence modeling for CFD*. La Cãnada (Calif.): DCW Industries.

Xiao, H., & Cinnella, P. (2019). Quantification of model uncertainty in RANS simulations: A review. *Progress In Aerospace Sciences*, *108*, 1-31. doi: 10.1016/j.paerosci.2018.10.001

Xu, C., Chen, L., & Lu, X. (2007). Large-Eddy and Detached-Eddy Simulations of the Separated Flow Around a Circular Cylinder. *Journal Of Hydrodynamics*, *19*(5), 559-563. doi: 10.1016/s1001-6058(07)60153-x

Yırtıcı, Ö. (2012). *Detached Eddy Sımulatıon Of Turbulent Flow On 2D Hybrıd Grıds* (published master's thesis). Middle East Technical University.

Zhang, J., Liang, D., Fan, X., & Liu, H. (2019). Detached eddy simulation of flow through a circular patch of free-surface-piercing cylinders. *Advances In Water Resources*, *123*, 96-108. doi: 10.1016/j.advwatres.2018.11.008

Zhang, J., Wang, X., Liang, D., & Liu, H. (2015). Application of detached-eddy simulation to free surface flow over dunes. Engineering Applications of Computational Fluid Mechanics, 9(1), 556-566. doi: 10.1080/19942060.2015.1092269

Zhou, L. (2018). *Theory and Modeling of Dispersed Multiphase Turbulent Reacting Flows* (1st ed.). Butterworth-Heinemann.